Optimization of ramified absorber networks doing desalination

Martin S. Singleton*
Center for Complex Systems Research, Department of Physics, University of Illinois at Urbana-Champaign, Urbana, Illinois 61801, USA

Gregor Heiss
Institut für physikalische Chemie, Ludwig-Maximilians-Universität München, DE-80539 München, Germany

Alfred Hübler
Department of Physics, University of Illinois at Urbana-Champaign, Urbana, IL 61801, USA

(Received 3 March 2010; revised manuscript received 12 September 2010; published 28 January 2011)

An iterated function system is used to generate fractal-like ramified graph networks of absorbers, which are optimized for desalination performance. The diffusion equation is solved for the boundary case of constant pressure difference at the absorbers and a constant ambient salt concentration far from the absorbers, while constraining both the total length of the network and the total area of the absorbers to be constant as functions of generation G. A linearized form of the solution was put in dimensionless form which depends only on a dimensionless membrane resistance, a dimensionless inverse svelteness ratio, and G. For each of the first nine generations $G = 2, \ldots, 10$, the optimal graph shapes were obtained. Total water production rate increases parabolically as a function of generation, with a maximum at $G = 7$. Total water production rate is shown to be approximately linearly related to the power consumed, for a fixed generation. Branching ratios which are optimal for desalination asymptote decreasingly to $r = 0.510$ for large G, while branching angles which are optimal for desalination asymptote decreasingly to 1.17 radians. Asymmetric graphs were found to be less efficient for desalination than symmetric graphs. The geometry which is optimal for desalination does not depend strongly on the dimensionless parameters, but the optimal water production does. The optimal generation was found to increase with the inverse svelteness ratio.

DOI: 10.1103/PhysRevE.83.016308 PACS number(s): 47.56.+r, 47.57.eb, 88.05.Gh, 87.19.lp

I. INTRODUCTION

Of the two most prevalent methods of desalination today, reverse osmosis and thermal distillation [1], reverse osmosis began relatively recently with the discovery in 1959 at University of California, Los Angeles, by Loeb and Sourirajan [2] of a chemically homogeneous, physically asymmetric porous cellulose acetate polymer film [3] which made reverse osmosis economically feasible. Since typical energy requirements of reverse osmosis of 2.2 kWh/m^3 [4] are a factor of 3 larger than the theoretical limit of 0.7 kWh/m^3, other methods such as forward osmosis [5], low-temperature thermal desalination [6], and membrane distillation [7] continue to be introduced as viable alternatives. The byproducts of desalination include brine and mineral salts. Since these are acutely harmful to the environment, systematic studies of desalination from a Gibbs free-energy perspective have become useful [8].

Current desalination research has continued to focus to a large extent on studying membranes. Promising results have been obtained from aquaporin [9] and carbon nanotube based membranes [10], while analytical studies have yielded models for porous ion transport [11] and ion-exchange membranes [12]. Molecular dynamics studies dealing with ion layers in solution [13,14] and osmosis through membranes [15–17] have also been popular. The optimality of fractal membranes [18,19] has also been investigated, and in this connection it has been shown that membranes can be seen to be equivalent to electrodes [20]. Fractal antennae [21,22] and battery electrodes [23] have also been shown to have optimal properties. It has been found that microscopic [24] and macroscopic [25] aggregates can spontaneously lead to ramified fractal networks, due to the optimality of the fractal configurations. Fractal growth networks which exhibit pattern formation under a reaction-diffusion dynamic have also been studied [26]. A useful mathematical description for the growth of fractal networks, iterated function systems [27], has been used to conveniently formalize and study visualization of fractals generated from chaotic sequences [28,29].

The study and construction of ramified fractal-like networks and optimization of transport properties in the networks has been well investigated by many researchers. One of the foundational concepts which grounds such investigation is the principle that structures in nature and engineering adapt themselves to optimally serve their functions. In one of the seminal works illustrating this principle, Murray [30] showed how the cost of blood volume was the determining factor for the radii of a network of vessels transporting oxygen in man. This has subsequently led to the development of the constructal theory [31] of optimal flow configurations as a branch of nonequilibrium thermodynamics. Xu and Yu have recently shown how the thermal conductivity of both fractal treelike branched networks [32] and of H-shaped fractal networks in composites [33] was significantly lower than that of conventional parallel channels. Similarly, Chen *et al.* [34] have elucidated optimal branching diameter ratios which enhanced the effective permeability of composites over comparably sized parallel networks. Scaling laws for transport properties of conductive, convective, laminar, and turbulent flow fractal networks have also been presented [32]. In related

*mssingle@uiuc.edu

work, Mauroy and others [35] have determined the flow asymmetry versus branching angle for different aspect ratios and Reynolds numbers in a fractal-like tree network. These works have contributed much toward our understanding of optimal constructal theory. We look at optimal desalination absorber networks. Our work is different from these earlier studies in that we have focused on the shapes themselves, unencumbered by the internal transport dynamics. In a sense we complement the previous work by helping impart a foundation for it. Furthermore, previous work has not shown how optimal constructions arose from adaptation by absorbing networks to diffusive environments.

In the following, we explore the optimal geometry for networks of absorbers in a diffusive medium, applying this to the important case of desalination. We start by providing an explanation of what the system looks like in Sec. II. In Sec. III, we use the formalism of the iterated function system to generate a set of ramified graph networks of absorbers. The diffusion equation is solved by analogy to electrostatics in Sec. IV, where we linearize the system and define the most relevant boundary condition to examine, that of constant pressure difference absorbers. In Sec. V we discuss the results, as well as nonsymmetric binary graphs, dependence of the solution on dimensionless parameters, and future research directions. Finally, in Sec. IV we summarize our results.

II. PHYSICAL SITUATION OF THE POSED PROBLEM

Although we present a more formally detailed account of the technical details of the posed problem in what follows, it will be useful to initially give a down-to-earth description of the physical situation. Our model is that of two planar, symmetric, binary trees, composed of a network of hollow pipes, joined at their base (see Fig. 1), imbedded in a volume of saline solution. At the ends of the tree there are spherically shaped membrane surfaces (red outline in Fig. 1), which are permeable to water. Within the network of pipes near the base there are two symmetrically situated pumps which will thus produce a constant pressure difference at the absorbers. This is the picture we have in mind. In order to better isolate the problem, we then dispense with the internal flow dynamics of the system, so that the the diameters of the pipes play no role in what follows. Our principal aim is to determine which branching angle, branching length ratio, and tree generation can most efficiently extract water from the pattern of salt concentration of the saline solution. In doing this we also make the further simplification that the saline solution has reached a steady state distribution of salt concentration.

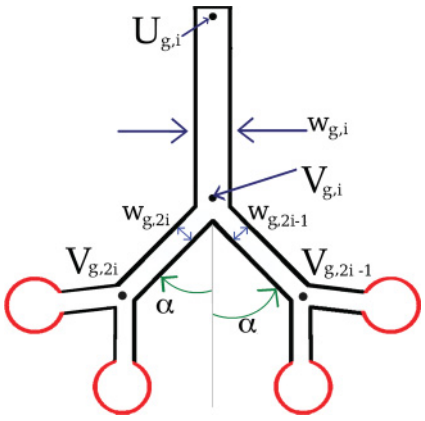

FIG. 1. (Color online) Schematic for a ramified network consisting of pipes with diameters $w_{g,i}$, where the angles, ratios, and diameters depend on the generation g. Red shading indicates effective membrane surface. For a network of total length l, $\mathbf{U}_{g,i}$ and $\mathbf{V}_{g,i}$ denote $l\mathbf{u}_{g,i}$ and $l\mathbf{u}_{g,i}$ respectively.

III. RAMIFIED GRAPHS AND ITERATED FUNCTION SYSTEMS

We use an iterated function system [27] which maps a set of 2^g line segments into a set with 2^{g+1} members:

$$\phi : S_g = \{A_{g,i}\} \longrightarrow S_{g+1} = \{A_{g+1,2i}, A_{g+1,2i-1}\},$$
$$g = 1, \ldots, G-1, i = 1, \ldots, 2^g, \tag{1}$$

where $A_{g,i} = \binom{\mathbf{u}_{g,i}}{\mathbf{v}_{g,i}}$ represents the line segment $\overline{\mathbf{u}_{g,i}\mathbf{v}_{g,i}}$ between nodes $\mathbf{u}_{g,i}$ and $\mathbf{v}_{g,i}$, and G is the total number of generations. The line segments of generation g are functions of the line segments of previous generations, that is: $A_{g+1,2i-1} = h_L(A_{g,i})$ and $A_{g+1,2i} = h_R(A_{g,i})$, where $h_{L,R}$ are linear transformations given in Appendix A, and $A_{1,1} = [0, \frac{1-2r}{1-(2r)^G}, 0]$ is the stem segment. The transformations $h_{L,R}$ depend parametrically on the ratio r between segments of generation $g+1$ and segments of generation g, and the angle α with which generation $g+1$ segments branch away from generation g segments. Note that by the definition of $A_{1,1}$ the total unitless length $A_G = \Sigma_{g=1}^{G} \Sigma_{i=1}^{2^{g-1}} |A_{g,i}|$ is kept fixed at 1 as G is varied, i.e., $A_G = 1$ for all G. The union of line segments forms a connected ramified graph $\mathcal{G}$:

$$\mathcal{G} = \bigcup_{\substack{i \leq 2^{g-1} \\ g \leq G}} A_{g,i},$$

such that the starting point of the line segment of generation $g+1$ is the endpoint of a line segment of generation g, i.e., $\mathbf{u}_{g+1,2i} = \mathbf{u}_{g+1,2i+1} = \mathbf{v}_{g,i}$. The transformation $h_{L,R}$ of Appendix A satisfies the relation $|\overline{\mathbf{u}_{g+1,2i+1}\mathbf{v}_{g+1,2i+1}}| = |\overline{\mathbf{u}_{g+1,2i}\mathbf{v}_{g+1,2i}}| = r \cdot |\overline{\mathbf{u}_{g,i}\mathbf{v}_{g,i}}|$; therefore, the iterated function is a contraction mapping for $0 \leqslant r < 1$. In what follows we assume that $0 \leqslant r < 1$. The graph $\mathcal{G}$ models a ramified network of linear conduits, such as pipes (see Fig. 2). If the total length of the network is l, we may define $\mathbf{U}_{g,i} = l\mathbf{u}_{g,i}$ and $\mathbf{V}_{g,i} = l\mathbf{v}_{g,i}$. The endpoints $S = \{\mathbf{V}_{G,i}\}$ are the locations of absorbers, and $\mathbf{U}_{1,1}$ is an outlet for the permeate. The absorbers are semipermeable membranes which use reverse osmosis or forward osmosis [36] to extract water from saltwater.

IV. SPATIAL DEPENDENCE OF THE SALT CONCENTRATION

By conservation of salt molecules in a diffusive medium we have the equation $\frac{\partial c}{\partial t} = -\nabla \cdot \mathbf{J}$, where c is the salt concentration in mol/m^3, and $\mathbf{J}$ is the flux of c. Using Fick's law,

$$\mathbf{J} = -D\nabla c, \tag{2}$$

where D is the diffusion coefficient in units of m^2/s. We thus find the diffusion equation for the system of water absorbers,

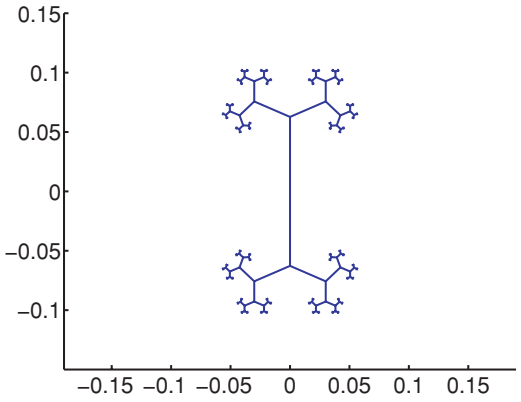

FIG. 2. (Color online) Ramified graph which is optimal for (i.e., it maximizes) water production occurs for $G = 7$, $r = 0.521$, and $\alpha = 1.16$. The graph is optimal in the sense that other graphs with the same length and total area of absorbers, but with different branching angles and branching ratios, have lower water production rates.

$\frac{\partial c}{\partial t} = -\nabla \cdot (-D\nabla c)$. Assuming that D is constant and that the system has reached a steady state, we get Laplace's equation:

$$D\nabla^2 c = 0. \tag{3}$$

In solving Eq. (3), we assume the following boundary conditions: (i) the water surface is insulating, i.e., $\mathbf{J}(x = 0) = 0$, (ii) as the distance from the ramified graph approaches infinity the concentration goes to an ambient concentration c_∞, and (iii) the endpoints $\{v_{G,i}\}$ of the ramified graph are the centers of small spherical absorbers with radii R_a which are sufficiently far apart that the salt concentration at the surface of each absorber is isotropic. Near an absorber i the salt concentration is given by:

$$c(\mathbf{r}) = \frac{s_i}{|\mathbf{r} - \mathbf{V}_{G,i}|} + c_{i,x}(x - x_i) + c_{i,y}(y - y_i) + c_i^*, \tag{4}$$

where s_i are integration constants with units of $\frac{\text{mol}}{\text{m}^2}$, $\mathbf{r} = (x, y)$ is the location of measurement of the concentration c, c_i^* is

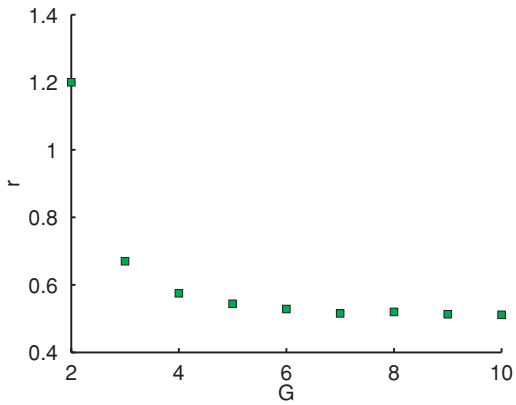

FIG. 3. (Color online) Ratio for ramified graph networks having maximal water output for the case of constant pressure difference absorbers as function of number of generations, for generations $G = 2$ to $G = 10$, with parameter values as in Table I. Ratios were deemed optimal if the corresponding water production rate was maximal over all angles.

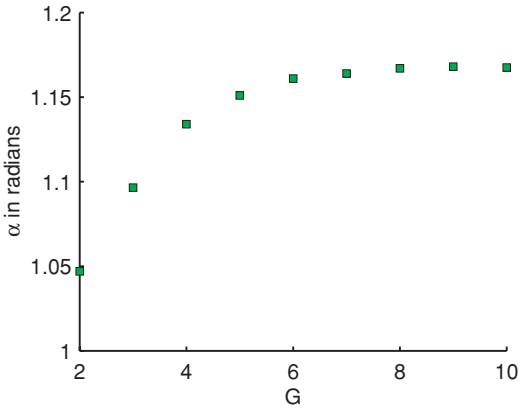

FIG. 4. (Color online) Angle for ramified graph networks having maximal water output for the case of constant pressure difference absorbers as function of number of generations, for generations $G = 2$ to $G = 10$, with parameter values as in Table I. Angles were deemed optimal if the corresponding water production rate was maximal over all ratios.

a constant, and $c_{i,x}$ and $c_{i,y}$ are first order derivatives which couple absorber i to the other absorbers in the network.

Using Gauss's law and integrating over a spherical region Ω of radius r centered at a single salt absorber of radius $r > R_a$, the production rate Q_i of salt in units of $\frac{\text{mol}}{\text{s}}$ coming from a single absorber i is given by:

$$Q_i = \int_{\partial\Omega} \mathbf{J} \cdot \hat{\mathbf{n}}\, dA = 4\pi D s_i, \tag{5}$$

where J is computed by applying Eq. (2) to Eq. (4). Gauss's law shows that the constant s_i is proportional to the salt production rate Q_i coming from a single absorber. Therefore, since Eq. (3) is linear, the principle of superposition gives an approximate complete solution to Eq. (3):

$$c_i = \frac{2^{G/2} Q_i}{D\sqrt{4\pi A_a}} + \frac{1}{4\pi D l} \sum_{j \neq i} \frac{Q_j}{|\mathbf{v}_{G,j} - \mathbf{v}_{G,i}|} + c_\infty, \tag{6}$$

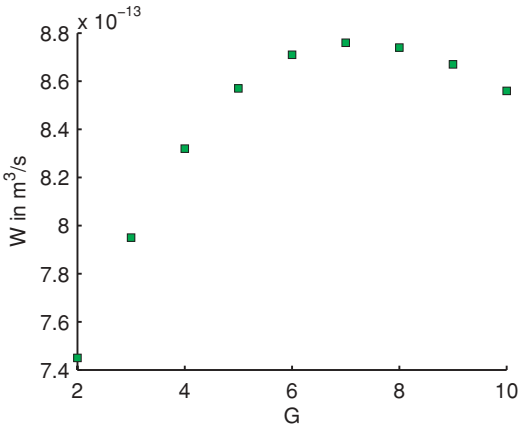

FIG. 5. (Color online) Optimal water production rates in m^3/s for ramified graph networks in the case of constant pressure difference absorbers as function of number of generations, for generations $G = 2$ to $G = 10$, with parameter values as in Table I. These are the values of water production per unit time that were maxima (and hence optimal) for each generation by independently varying ratios and angles.

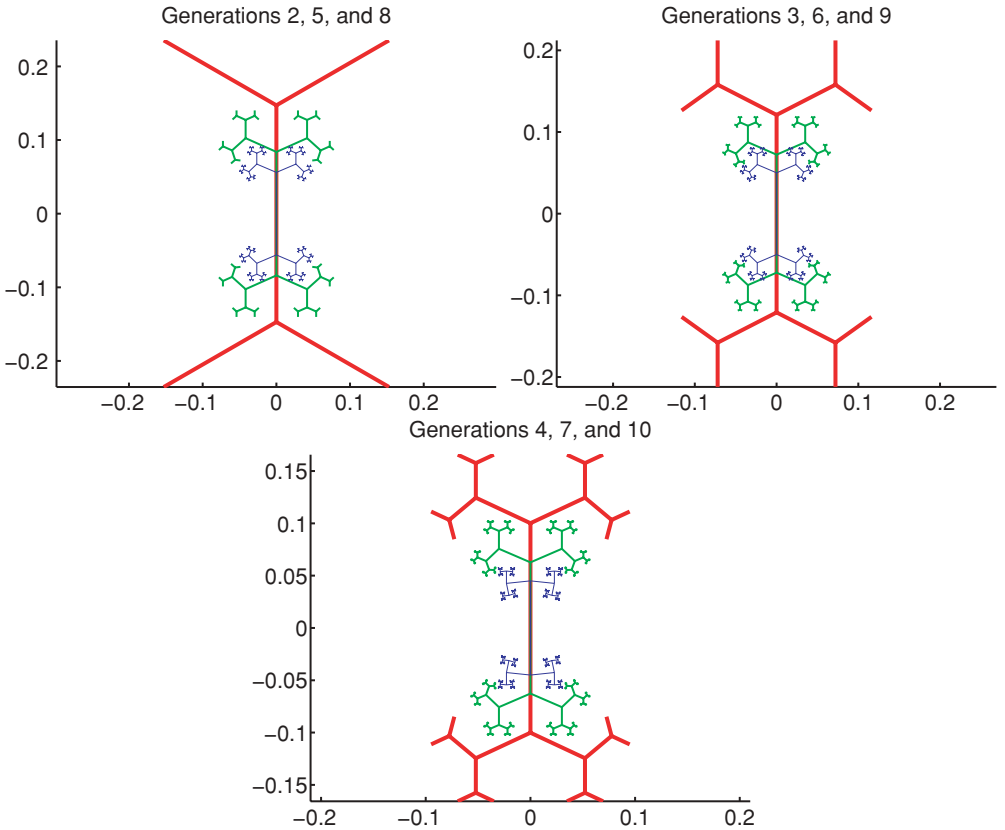

FIG. 6. (Color online) Ramified graphs having optimal properties (maximal water production rate for constant pressure difference absorbers) as in Figs. 3 and 4 for generations $G = 2$ to $G = 10$. The graphs are optimal in the sense that other graphs with the same length and total area of absorbers, but with different branching angles and branching ratios, have lower water production rates.

where c_i is defined as the salt concentration at the ith absorber, $i = 1, \ldots, 2^G$, and $A_a = 2^G 4\pi R_a^2$ is the total surface area of the absorbers.

The salt concentration c_i at the outside of the membrane of absorber i depends on the applied pressure drop Δ_i at each absorber membrane. In what follows, we consider the case where $\Delta_i = \Delta$ is fixed for all i, which is physically the most easily realized case. The pressure difference across the membrane Δ is the sum of the osmotic pressure and the membrane flow resistance Δ_m,

$$\begin{aligned}\Delta &= (c_i - c_0)RT + \Delta_m \\ &= c_i' RT + \Delta_m, \end{aligned} \tag{7}$$

where c_0 is the salt concentration inside the absorber, $c_i' = c_i - c_0$ is the difference in concentration from outside to inside the absorber, and $\Delta_m = \frac{W_i \mu b}{4\pi\kappa R_a^2}$ is the membrane flow resistance. Here the water production rate W_i is the volume of water flow through absorber i per unit time, μ is the viscosity of the medium in $\mathrm{kg\,m^{-1}\,s^{-1}}$, κ is the membrane permeability in m^2, b is the thickness of the membrane, $R = 8.314$ J/K mol is the ideal gas constant, and T is the temperature in Kelvins. By the stoichiometry of the molecules which interact with the absorbers, the rate of water production W_i at node i is given by the relation

$$Q_i = W_i c_i', \tag{8}$$

where Q_i is the salt production rate of node i. Hence the total rate of water production W for the absorber network is

$$W = \sum_{i=1}^{2^G} \frac{Q_i}{c_i'}. \tag{9}$$

By solving Eq. (7) for W_i, the power consumption $P_i = \Delta W_i$ at absorber i is

$$P_i = (c_i' RT + \Delta_m) W_i, \tag{10}$$

and the energy consumption $E_i = P_i / W_i$ is given by:

$$\begin{aligned} E_i &= c_i' RT + \Delta_m \\ &= \Delta, \; i = 1, \ldots, 2^G. \end{aligned} \tag{11}$$

Using Eqs. (7) and (8), the salt production rate Q_i is given by an expression quadratic in c_i':

$$Q_i = \frac{\kappa A_a}{\mu b 2^G}\left(c_i'\Delta - {c_i'}^2 RT\right). \tag{12}$$

Substituting these expressions for Q_i into Eq. (6) then gives a quadratic form in the c_i':

$$\begin{aligned} &\frac{\mu b D}{\kappa}(c_\delta - c_i') + \sqrt{\frac{A_a}{2^G 4\pi}}\left(c_i'\Delta - {c_i'}^2 RT\right) \\ &+ \frac{A_a}{2^G 4\pi l} \sum_{j \neq i} \frac{c_j'\Delta - {c_j'}^2 RT}{|\mathbf{v}_{G,j} - \mathbf{v}_{G,i}|} = 0, \end{aligned} \tag{13}$$

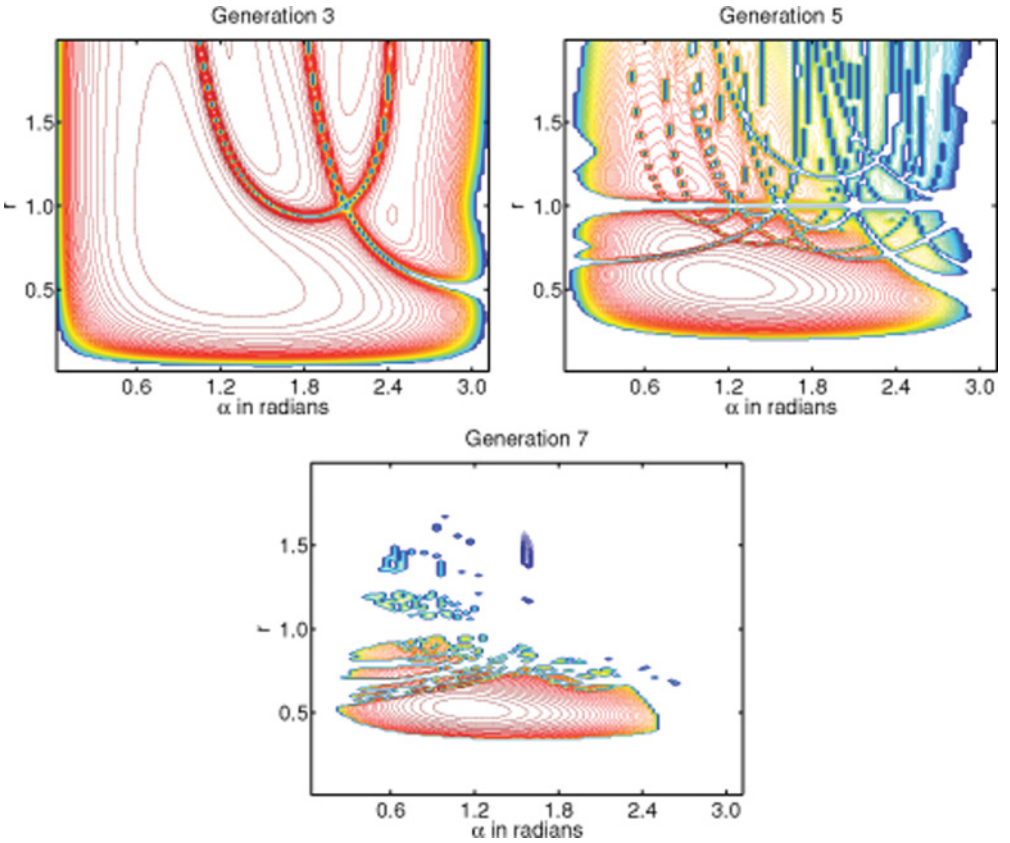

FIG. 7. (Color online) Contours of total water production for constant pressure difference absorbers over the ramified graph network for equal increments of angles between 0 and π, and ratios of 0 to .9, for generations $G = 3, 5$, and 7, with parameter values as in Table I.

where $c_\delta = c_\infty - c_0$ is the difference in salt concentration between the inside of the absorber and infinity. Eq. (13) constitutes our steady state solution of the diffusion equation for the boundary case of constant pressure difference at the absorbers and a constant ambient salt concentration far from the absorbers. We provide more details of our procedure for this solution, which follows the analogy of diffusion to electrostatics originated by Maxwell [37], in Appendix B.

Defining a dimensionless concentration

$$\tilde{c}_i = \frac{c_i' - \frac{\Delta}{RT}}{c_\delta - \frac{\Delta}{RT}}, \tag{14}$$

Eq. (13) may be rewritten in dimensionless form as

$$\tilde{c}_i + \frac{k}{\sqrt{4\pi 2^G}}\tilde{c}_i(1-\xi\tilde{c}_i) + \frac{k\beta}{4\pi 2^G}\sum_{j\neq i}\frac{\tilde{c}_j(1-\xi\tilde{c}_j)}{|\mathbf{v}_{G,j}-\mathbf{v}_{G,i}|} = 1, \tag{15}$$

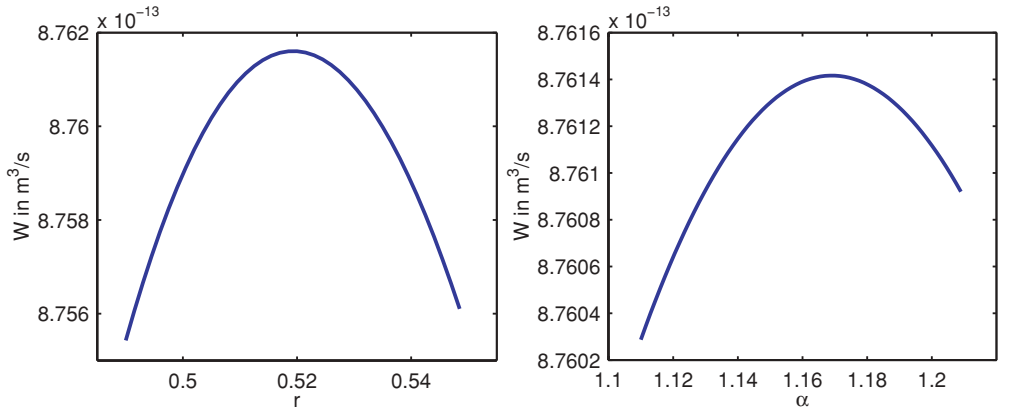

FIG. 8. (Color online) Plots of water production W vs ratio r with $G = 7$ and $\alpha = 1.167$ (left), and water production W vs angle α with $G = 7$ and $r = 0.5155$ (right).

where the dimensionless parameters of the problem are

$$k = \frac{\sqrt{A_a}\kappa\Delta}{\mu b D}, \tag{16}$$

$$\beta = \frac{\sqrt{A_a}}{l}, \tag{17}$$

$$\xi = \frac{\Delta - c_\delta RT}{\Delta}, \tag{18}$$

and G. We observe that each of these dimensionless parameters has a physical interpretation. The parameter k is an effective dimensionless membrane resistance which relates the applied pressure induced resistive flow across the membrane to the diffusivity D of the medium, β is an inverse svelteness ratio which gives how large the fixed total absorber area A_a is in relation to the fixed total length l, and ξ is the normalized applied pressure. From Eqs. (8) and (12), we can then write the rate of water production W_i for node i as

$$W_i = \frac{lDk\beta\xi}{2^G}\tilde{c}_i. \tag{19}$$

For typical desalination values given in Table I, on average $\xi\tilde{c}_j < .03$ for generations up to $G = 10$. Therefore, Eq. (15) can be linearized with a Taylor series expansion about $\tilde{c}_i = 0$ (see Appendix C):

$$\left(1 + \frac{k}{\sqrt{4\pi 2^G}}\right)\tilde{c}_i + \frac{k\beta}{4\pi 2^G}\sum_{j\neq i}\frac{\tilde{c}_j}{|\mathbf{v}_{G,j} - \mathbf{v}_{G,i}|} = 1. \tag{20}$$

In order to maximize the total water production rate W, given the fixed applied pressure Δ, the system given by Eq. (20) must be solved. Levy's theorem [38] suggests that a solution exists (see Appendix D) except when absorbers overlap. Figure 2 shows the ramified graph corresponding to the ramified network which is optimal for water production rate, since for all angles and ratios considered it has the largest water production rate. In all cases for the values given in Table I, the error made by neglecting the second order term (C6), which we take as the ratio of the Euclidean norm of the second order term vector to the Euclidean norm of the first order term vector [see Eq. (C5)], was less than 6×10^{-3}.

V. DISCUSSION

In our study we seek to explore morphologies which produce maximal water production rates. Since a desalination system is considered most desirable if it maximizes water production (*ceteris paribus*), we thus term graphs possessing this quality "optimal." The optimal ratios and angles, respectively, as functions of generation corresponding to the optimal ramified graphs are given in Figs. 3 and 4. By varying angle and ratio independently and calculating the water production for each generation, we were able to find the optimal ratios and angles in the sense that they maximized water production rates. By fitting the optimal ratio and angle plots, we were able to evaluate their asymptotic values. In Fig. 3 it is demonstrated that the optimal ratio decays asymptotically to the value 0.510, which as an approximation to 0.5 is the value one might expect based upon symmetry considerations. Figure 4 shows that the optimal branching angles asymptote exponentially to the value 1.17, which is about 67°. In Fig. 5 we give the optimal water production rates as a function of generation. The criterion for optimization was that the graph produced the maximum volume of water per unit time. Hence Fig. 5 plots the actual maxima that were found by varying ratio and angle as generation G was varied. Figure 5 shows that the optimal water production increases up to a maximum at about $G = 71$. In Fig. 6 are given all the optimal graphs for generations $G = 2$ to $G = 10$. For clarity, we superimpose the graphs in groups of three. Plotting graphs three generations apart on the same plot (e.g., generations 2, 5, and 8) enables one to distinguish the features of each individual graph better (as opposed to, e.g., plotting generations 2, 3, and 4 together). For each separate graph, we apply the iterated function system with inputs for the specified generation G, and the optimal ratio r and angle α for that generation. The lengths of all these nine graphs are the same. The optimal ratios and angles are those values which yield the maximum water production for the corresponding desalination system.

Figure 7 shows contours of the total water production rate of the desalination system versus angle and ratio for generations 3, 5, and 7. It is noteworthy from the contour plots of water production of Fig. 7 that as generation $G = 7$ is reached, the possible solutions to the system become increasingly spatially restricted (the maximum is sharp), so that by generation $G = 10$ the system is solvable (see Appendix D) for only a low percentage of cases. It is evident from the contour plots that the optimal water production which occurs at about generation

TABLE I. Typical desalination values used to solve Eq. (3).

Desalination parameter	Typical value
D	10^{-9} m^2/s
T	290 K
c_δ	564 mol/m^3
Δ	1.4×10^6 Pa
$\frac{\kappa}{\mu}$	9.72×10^{-20} m^3 s/kg
A_a	.00025 m^2
b	10^{-6} m
l	1.0 m

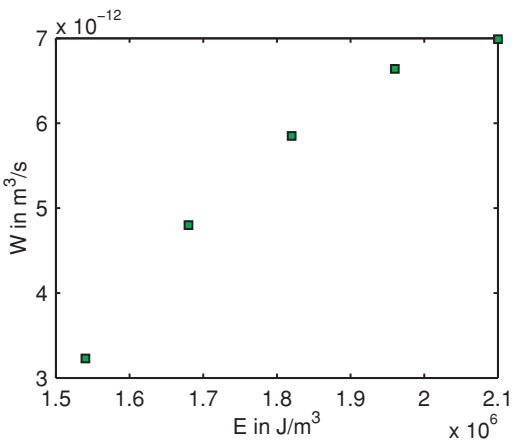

FIG. 9. (Color online) Optimal water production rate in m^3/s for $G = 7$ as a function of the energy consumption per volume E of permeate produced.

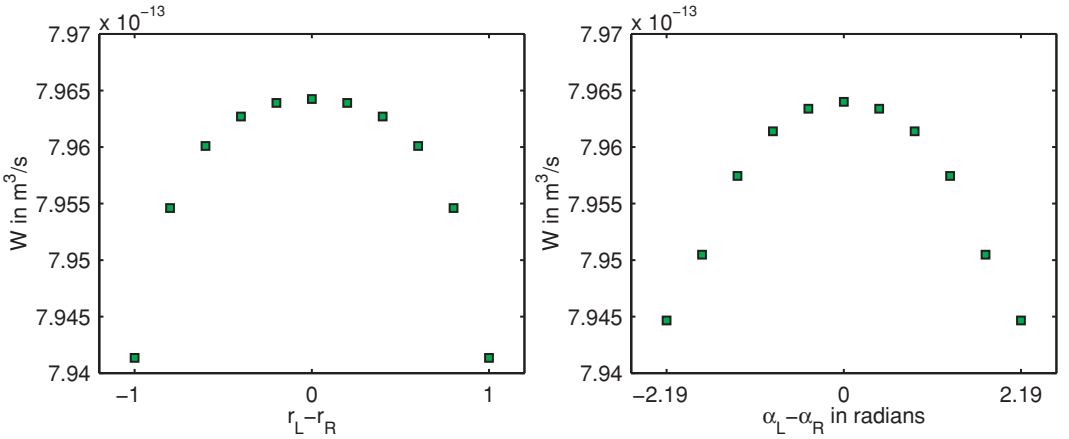

FIG. 10. (Color online) Optimal water production for $G = 3$ vs ratio difference (left) and angle difference (right). For the ratio difference plot, alpha was the optimal angle, and ratios were varied independently about the optimal ratio. For the angle difference plot, ratio was the optimal ratio, and angles were varied independently about the optimal angle.

$G = 7.1$ is a type of local maximum. Taking cross-sections through the maximum by holding either the branching angle or branching ratio constant at their optimal values it is possible to determine how the water production changes as a function of angle or ratio. This behavior is found to be parabolic in both cases, as depicted in Fig. 8, which also enables us to determine at which angle and length ratio the water production rate can reach the maximum value. In Fig. 9 the relation between the optimal total water production rate W and the energy consumption of the desalination nodes, given by Eq. (11), is shown to be a nearly linear, increasing function.

Previous work has shown that termini of ramified transportation networks are binary [25], so we have restricted our investigation to binary graphs. It may be suggested that only a special case of binary graphs has been examined, and that the class of binary graphs may have other more optimal geometries than our solutions. However, we argue that the symmetric binary graphs generated by the iterated function system of Eq. (A1) yield the optimal geometries among more general binary graphs, as is suggested by the most symmetric asymptotic optimal ratios and angles of the results. Indeed, we varied the difference in branching ratio in the range $-1 \leqslant r_L - r_R \leqslant 1$ while keeping the branching angle fixed at the optimal angle for $G = 3$, and found that the optimal water production occurred when $r_L - r_R = 0$, which is the case of our symmetric binary graph (Fig. 10 left). We similarly changed the branching angle in the range of $-2.19 \leqslant \alpha_L - \alpha_R \leqslant 2.19$ with branching ratio kept at the optimal value for $G = 3$, and found that the symmetric binary graphs $\alpha_L - \alpha_R = 0$ produced the greatest water production (Fig. 10 right). Thus our results also suggest (although this verification is by no means exhaustive) that the symmetric types of binary graphs which Eq. (A1) generates have the most optimal properties.

Another modification in the assumptions which conceivably might change our results is to alter one or more of the parameters of the problem. In order to eliminate any dependence on scale, only dimensionless parameters of the problem should be changed. Referring to the linear system of Eq. (20), we have the two dimensionless parameters β and k, given by Eqs. (17) and (16), respectively. Evaluating Eq. (17) and Eq. (16) with the typical values given in Table I gives $\beta = .0158$ and k = 2.15. If we thus define $\beta_0 = .0158$ and $k_0 = 2.15$, we see that β_0 and k_0 signify the typical values of the dimensionless parameters β and k. Defining $\beta_d = d\beta_0$ and $k_d = dk_0$, we then studied the solutions to the linear system of

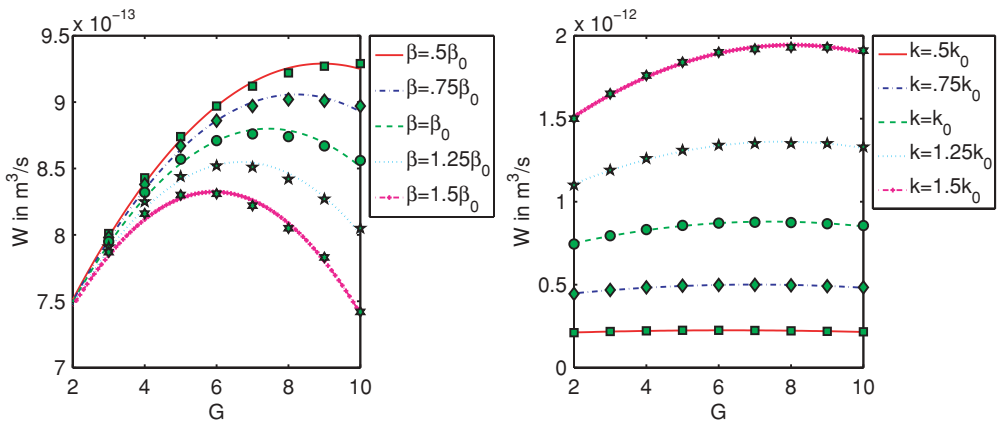

FIG. 11. (Color online) Curve fits of optimal water production while varying independent dimensionless parameters. Left: Effect of varying β. Right: Effect of varying k. All curves were fitted to the general parabolic form of $W(G) = C_1 - C_2(G - G_{\max})^2$.

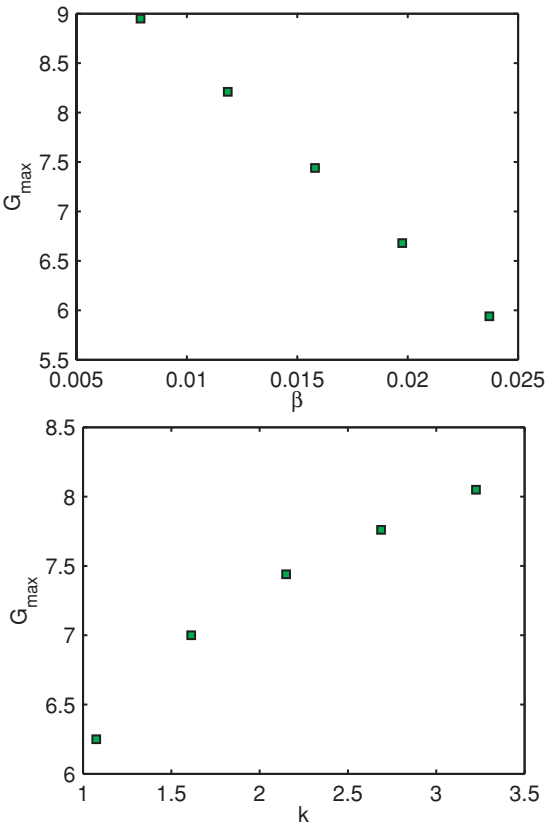

FIG. 12. (Color online) Dependence of $G_{\max}$ from Eq. (21) on the dimensionless parameters β (top) and k (bottom).

Eq. (20) by alternately holding $k = k_0$ constant with $\beta = \beta_d$ varying, and then $\beta = \beta_0$ constant while varying $k = k_d$. In each case d was varied between .5 and 1.5, in steps of .25. Perhaps not so surprisingly in light of our systematic study of the dependence of optimality on geometry earlier, the optimal ratios and angles did not change for these different values of (β,k). However, the optimal water production rates did change. In order to see this, we produced curve fits for the optimal water production plots (e.g., for plots like that of Fig. 5) by the function

$$W(G) = C_1 - C_2(G - G_{\max})^2. \tag{21}$$

For all of the different parameter combinations of (β,k) the maximal water output was found to have an inverted parabolic dependence on the generation G, as shown by the curves in Fig. 11. In fact, the value of $G_{\max}$ gives by extrapolation a value for the optimal (in the sense of maximal water production) generation. Thus although the parameters β and k do not appear explicitly in Eq. (21), it is shown in Fig. 12 how the optimal generation $G_{\max}$ of Eq. (21) changes as the parameters β and k are varied. Indeed, Fig. 12 demonstrates how $G_{\max}$ has an increasing (implicit) dependence on k, while $G_{\max}$ decreases with increasing β. This shows that smaller absorbers favor a higher generation.

VI. CONCLUSION

Beginning with an iterated function system which was used to generate the ramified graph networks of absorbers (Fig. 1), the diffusion equation was solved using the analogy to electrostatics. After introducing dimensionless parameters which had direct physical correlates, the system was linearized for the case of constant pressure difference absorbers, experimentally the most accessible case. The linear system of 2^G equations was then solved for the 2^G unknowns, specifying the concentrations about each of the 2^G absorbers in the network, for generations $G = 2$ to $G = 10$ while independently varying branching ratios and angles. The optimal ramified graph, which resulted in the greatest water production rate, all other quantities being equal, is shown in Fig. 2. Optimal ratios, angles, and water production rates were obtained for each generation G. Contour plots showed how the solutions smoothly approached the same optimum as G was increased, thus demonstrating that information was not lost as the system grew in size and became less soluble (see Appendix D). By independently varying the left and right branching angles and ratios, it was shown why our symmetric ramified graphs were preferable to the asymmetric variants from the point of view of optimization. Changing the values of the independent dimensionless parameters demonstrated that the geometry of the optimal graphs did not change, but that the optimal generation decreased as the scaling factor increased. The findings we present here also show that the smaller the absorber area, the higher the optimal generation. The foregoing may help design more efficient networks and provide optimal shapes for practical desalination systems to increase the supply of drinking water in the world.

ACKNOWLEDGMENTS

The authors acknowledge useful conversations with Davit Sivil, John Cheeseman, and Rhanor Gillette. Special thanks to our graphic artist, Kyram Singleton. The authors gratefully acknowledge the support for this work by Defense Advanced Research Projects Agency (DARPA) Physical Intelligence subcontract (HRL9060-000706).

APPENDIX A: ITERATED FUNCTION SYSTEM LINEAR TRANSFORMATION

$$h_{L/R} = \begin{pmatrix} 0 & 0 & 0 & 1 & 0 & 0 \\ 0 & 0 & 0 & 0 & 1 & 0 \\ 0 & 0 & 0 & 0 & 0 & 0 \\ -r\cos\alpha & \pm r\sin\alpha & 0 & r\cos\alpha + 1 & \mp r\sin\alpha & 0 \\ \mp r\sin\alpha & -r\cos\alpha & 0 & \pm r\sin\alpha & r\cos\alpha + 1 & 0 \\ 0 & 0 & 0 & 0 & 0 & 0 \end{pmatrix}, \tag{A1}$$

APPENDIX B: ELECTROSTATIC ANALOGY TO DIFFUSION

Since we assume a steady state for Eq. (2), we are in essence solving Eq. (3). Since the Cauchy problem for an elliptical partial differential equation with an analytic right-hand side has a unique solution, we need only show that our general form of the solution of Eq. (6) is a solution to Eq. (3), and that the boundary conditions are satisfied. In electrostatics, the

solutions to Laplace's equation are the potential, with terms like $V_q = \frac{q}{4\pi\epsilon_0 r}$. By making the correspondences

$$\begin{aligned} q &\longrightarrow Q_i, \\ \epsilon_0 &\longrightarrow D, \\ V_q &\longrightarrow c_i, \end{aligned}$$

we get terms of the form given in Eq. (6). The first term on the right-hand side, $\frac{Q_i}{4\pi D R_a}$, is the contribution from absorber i to the concentration on the surface of node i, which is constant. The third term on the right-hand side, c_∞, is the constant background concentration. Far away from any absorbers the equivalent form of the solution will go to c_∞ since the other terms are inversely proportional to r, the distance to any given absorber (in the more general case the first term will also vary with distance from the center of node i). It only remains to show that the terms in the mixed sum (over j with i fixed) satisfy Laplace's equation. A generic summand of the sum is proportional to a function like

$$g(x,y,z) = \frac{1}{\sqrt{(a-x)^2+(b-y)^2+z^2}}, \tag{B1}$$

taking $x_i = a$, $y_i = b$ both constant, x and y the j variables, and recalling that the concentration is also a function of z (although since the desalination graphs we study are planar, in effect we set $z = 0$ in our solutions). Taking the Laplacian of g gives

$$\begin{aligned} \nabla^2 g = &\frac{3(a-x)^2}{[(a-x)^2+(b-y)^2+z^2]^{5/2}} \\ &+ \frac{3(b-y)^2}{[(a-x)^2+(b-y)^2+z^2]^{5/2}} \\ &+ \frac{3z^2}{[(a-x)^2+(b-y)^2+z^2]^{5/2}} \\ &- \frac{3}{[(a-x)^2+(b-y)^2+z^2]^{3/2}} \\ = &\ 0, \end{aligned} \tag{B2}$$

which demonstrates that Eq. (6) is a solution of Laplace's equation. The development of the boundary condition constant pressure difference at the absorbers is given earlier and gives Eq. (13) starting from Eq. (6). This completes the detailed account of our procedure for solution of the diffusion equation for the case of constant pressure difference at the absorbers and a constant ambient salt concentration far from the absorbers.

APPENDIX C: EXPANSION ABOUT $c_i' = \frac{\Delta}{RT}$

We want to apply Taylor's rule to the function

$$\begin{aligned} f_i(\tilde{c}_1,\tilde{c}_2,\ldots,\tilde{c}_{2^G}) = &\ \tilde{c}_i + \frac{k}{\sqrt{4\pi 2^G}}\tilde{c}_i(1+\xi\tilde{c}_i) \\ &+ \frac{k\beta}{4\pi 2^G}\sum_{j\neq i}\frac{\tilde{c}_j(1+\xi\tilde{c}_j)}{|\mathbf{v}_{G,j}-\mathbf{v}_{G,i}|}. \end{aligned} \tag{C1}$$

The first order Taylor series approximation to $f_i(\tilde{c})$ about $\tilde{c} = 0$ is

$$f_i(\tilde{c}) = f_i(0) + \sum_{j=1}^{2^G}\frac{\partial f_i}{\partial \tilde{c}_j}(0)\tilde{c}_j. \tag{C2}$$

Then, since

$$\begin{aligned} f_i(0) &= 0, \\ \frac{\partial f_i}{\partial \tilde{c}_i}(0) &= 1 + \frac{k}{\sqrt{4\pi 2^G}}, \\ \frac{\partial f_i}{\partial \tilde{c}_{j\neq i}}(0) &= \frac{k\beta}{4\pi 2^G|\mathbf{v}_{G,j}-\mathbf{v}_{G,i}|}, \end{aligned} \tag{C3}$$

$$\begin{aligned} \frac{\partial^2 f_i}{\partial \tilde{c}_i^2}(0) &= \frac{2k\xi}{\sqrt{4\pi 2^G}}, \\ \frac{\partial^2 f_i}{\partial \tilde{c}_i^2}(0) &= \frac{2k\beta\xi}{4\pi 2^G|\mathbf{v}_{G,j}-\mathbf{v}_{G,i}|}, \\ \frac{\partial^2 f_i}{\partial \tilde{c}_{k\neq j}\partial \tilde{c}_j}(0) &= 0, \end{aligned} \tag{C4}$$

we find Eq. (20):

$$\begin{aligned} f_i(\tilde{c}_i) \simeq &\left(1 + \frac{k}{\sqrt{4\pi 2^G}}\right)\tilde{c}_i \\ &+ \frac{k\beta}{4\pi 2^G}\sum_{j\neq i}\frac{\tilde{c}_j}{|\mathbf{v}_{G,j}-\mathbf{v}_{G,i}|} = 1, \end{aligned} \tag{C5}$$

with the neglected nonlinear term being

$$\begin{aligned} &\frac{1}{2}\sum_{k=1}^{2^G}\sum_{j=1}^{2^G}\frac{\partial^2 f_i}{\partial \tilde{c}_k\partial \tilde{c}_j}(0)\tilde{c}_k\tilde{c}_j \\ &\quad = \frac{k\xi}{\sqrt{4\pi 2^G}}\tilde{c}_i^2 + \frac{k\beta\xi}{4\pi 2^G}\sum_{j\neq i}\frac{\tilde{c}_j^2}{|\mathbf{v}_{G,j}-\mathbf{v}_{G,i}|}. \end{aligned} \tag{C6}$$

APPENDIX D: SUFFICIENT CONDITION FOR SOLUTION

Eq. (20) has a unique solution if the linear system is nonsingular. Writing the matrix A of coefficients of the system,

$$\begin{aligned} A &= \begin{pmatrix} 1+k & \frac{R_a k}{l|\mathbf{v}_{G,2}-\mathbf{v}_{G,1}|} & \cdots & \frac{R_a k}{l|\mathbf{v}_{G,2^G}-\mathbf{v}_{G,1}|} \\ \frac{R_a k}{l|\mathbf{v}_{G,1}-\mathbf{v}_{G,2}|} & 1+k & \cdots & \frac{R_a k}{l|\mathbf{v}_{G,2^G}-\mathbf{v}_{G,2}|} \\ \vdots & \vdots & \vdots & \vdots \\ \frac{R_a k}{l|\mathbf{v}_{G,1}-\mathbf{v}_{G,2^G}|} & \cdots & \cdots & 1+k \end{pmatrix} \\ &= \frac{k}{l}\begin{pmatrix} l\frac{1+k}{k} & \frac{R_a}{|\mathbf{v}_{G,2}-\mathbf{v}_{G,1}|} & \cdots & \frac{R_a}{|\mathbf{v}_{G,2^G}-\mathbf{v}_{G,1}|} \\ \frac{R_a}{|\mathbf{v}_{G,1}-\mathbf{v}_{G,2}|} & l\frac{1+k}{k} & \cdots & \frac{R_a}{|\mathbf{v}_{G,2^G}-\mathbf{v}_{G,2}|} \\ \vdots & \vdots & \vdots & \vdots \\ \frac{R_a}{|\mathbf{v}_{G,1}-\mathbf{v}_{G,2^G}|} & \cdots & \cdots & l\frac{1+k}{k} \end{pmatrix}. \end{aligned} \tag{D1}$$

According to a theorem due originally to L. Levy [38] on invertibility of matrices, A will be invertible if it is diagonally

dominant, i.e., it suffices that

$$l\frac{1+k}{k} > R_a \sum_{i\neq j} \frac{1}{|\mathbf{v}_{G,j} - \mathbf{v}_{G,i}|} \tag{D2}$$

holds for all $i = 1, \ldots, 2^G$. Let

$$\gamma_i = \sum_{i\neq j} \frac{1}{|\mathbf{v}_{G,j} - \mathbf{v}_{G,i}|}, \tag{D3}$$

then define $\gamma_{\max} = \max_{i=1,\ldots,2^G} \gamma_i$. Since Eq. (D2) is then satisfied if

$$\frac{l(1+k)}{R_a k} > \gamma_{\max}, \tag{D4}$$

we thus arrive at the form

$$\max_{i=1,\ldots,2^G} \left\{ \sum_{i\neq j} \frac{1}{|\mathbf{v}_{G,j} - \mathbf{v}_{G,i}|} \right\} < \frac{l(1+k)}{k} \sqrt{\frac{4\pi 2^G}{A_a}}. \tag{D5}$$

[1] R. F. Service, Science **313**, 1088 (2006).
[2] S. Loeb and S. Sourirajan, Adv. Chem. Ser. **38**, 117 (1963).
[3] R. L. Riley, U. Merten, and J. O. Gardner, Desalination **1**, 30 (1966).
[4] M. A. Shannon, P. W. Bohn, M. Elimelech, J. G. Georgiadis, B. J. Marinas, and A. M. Mayes, Nature (London) **452**, 301 (2008).
[5] M. Elimelech, Membr. Technol. **2007**, 7 (2007).
[6] Y. Bhattacharjee, Science **316**, 1837 (2007).
[7] Q. Schiermeier, Nature (London) **452**, 260 (2008).
[8] K. S. Spiegler and Y. M. El-Sayed, Desalination **134**, 109 (2001).
[9] M. Kumar, M. Grzelakowski, J. Zilles, M. Clark, and W. Meier, Proc. Natl. Acad. Sci. **104**, 20719 (2007).
[10] B. Corry, J. Phys. Chem. B **112**, 1427 (2008).
[11] T. Chou, Phys. Rev. Lett. **80**, 85 (1998).
[12] I. Rubinstein, B. Zaltzman, and T. Pundik, Phys. Rev. E **65**, 041507 (2002).
[13] L. Vrbka and P. Jungwirth, Phys. Rev. Lett. **95**, 148501 (2005).
[14] F. Zhu, E. Tajkhorshid, and K. Schulten, Phys. Rev. Lett. **93**, 224501 (2004).
[15] K. Leung, S. B. Rempe, and C. D. Lorenz, Phys. Rev. Lett. **96**, 095504 (2006).
[16] A. V. Raghunathan and N. R. Aluru, Phys. Rev. Lett. **97**, 024501 (2006).
[17] A. V. Raghunathan and N. R. Aluru, Phys. Rev. E **76**, 011202 (2007).
[18] C. M. Tam and A. Y. Tremblay, Desalination **90**, 77 (1993).
[19] M. S. Suwandi and M. S. Lefebvre, Desalination **70**, 225 (1988).
[20] P. Meakin and B. Sapoval, Phys. Rev. A **43**, 2993 (1991).
[21] Y. Kim and D. L. Jaggard, Proc. IEEE **74**, 1278 (1986).
[22] J. Anguera, C. Puente, E. Martínez, E. Rozan, Microwave Opt. Technol. Lett. **36**, 102 (2003).
[23] B. Y. Park, R. Zaouk, C. Wang, and M. Madou, J. Electrochem. Soc. **154**, P1 (2007).
[24] I. Lee, J. S. Ahn, and T. R. Hendricks, Langmuir **20**, 2478 (2004).
[25] J. K. Jun and A. H. Hubler, Proc. Natl. Acad. Sci. USA **102**, 536 (2005).
[26] K. Tucci and M. G. Cosenza, Physica D **199**, 91 (2004).
[27] M. F. Barnsley and S. Demko, Proc. R. Soc. London A **399**, 243 (1985).
[28] J. C. Sprott, Comput. Graphics **18**, 417 (1994).
[29] D. Ashlock and J. Golden, Physica D **181**, 274 (2003).
[30] C. D. Murray, Proc. Natl. Acad. Sci. USA **12**, 207 (1926).
[31] A. Bejan and S. Lorente, Appl. Phys. Rev. **100**, 041301 (2006).
[32] P. Xu and B. Yu, Sov. J. Appl. Phys. **100**, 104906 (2006).
[33] B. Yu and B. Li, Phys. Rev. E **73**, 066302 (2006).
[34] J. Chen, B. Yu, P. Xu, and Y. Li, Phys. Rev. E **75**, 056301 (2007).
[35] B. Mauroy, M. Filoche, J. S. Andrade Jr., and B. Sapoval, Phys. Rev. Lett. **90**, 148101 (2003).
[36] T. Y. Cath, A. E. Childress, and M. Elimelech, J. Membr. Sci. **281**, 70 (2006).
[37] J. E. McDonald, Z. Angew, Math. Phys. **14**, 610 (1963).
[38] O. Taussky, Am. Math. Mon. **56**, 672 (1949).